than it would be if the ocean circulation remained constant (-139 Pg C in 2 $\times$ CO_2 simulation and -497 Pg C in the 4 $\times$ CO_2 simulation), and it has an uncertainty of plus or minus several hundred petagrams because of our limited understanding of the biological response.

REFERENCES AND NOTES

1. K. P. Shine, Y. Fouquart, V. Ramaswamy, S. Solomon, J. Srinivasan, in *Climate Change 1994*, J. T. Houghton *et al.*, Eds. (Cambridge Univ. Press, Cambridge, 1995), pp. 161–203.
2. I. G. Enting, T. M. L. Wigley, M. Heimann, *Assessment of the IPCC CO_2 Modelling Study* (Division of Atmospheric Research, Commonwealth Scientific and Industrial Research Organisation, Aspendale, Victoria, Australia, 1994).
3. J. L. Sarmiento, C. Le Quéré, S. W. Pacala, *Global Biogeochem. Cycles* **9**, 121 (1995).
4. D. Schimel *et al.*, in (1), pp. 35–71.
5. S. Manabe and R. J. Stouffer, *Nature* **364**, 215 (1993).
6. _____, *J. Clim.* **7**, 5 (1994).
7. The atmospheric and oceanic models have a latitudinal spacing of 4.5°, and the longitudinal spacing is 3.75° in the oceanic model and 7.5° in the atmospheric model. The ocean has 12 vertical levels, and the atmosphere has nine. Simple models of sea ice and terrestrial heat and water budgets are also incorporated. The two GCMs were initialized independently using seasonal solar insolation and observed ocean surface temperature and salinity to force them until a steady-state was achieved. We minimized the drift that occurs upon coupling the models by adjusting the fluxes of heat and water by an amount that varied with region and season but remained constant throughout the global warming scenarios [S. Manabe, R. J. Stouffer, M. J. Spelman, K. Bryan, *J. Clim.* **4**, 785 (1991)].
8. J. T. Houghton, G. J. Jenkins, J. J. Ephraums, Eds., *Climate Change, The IPCC Scientific Assessment* (Cambridge Univ. Press, New York, 1990).
9. L. D. D. Harvey, *J. Geophys. Res.* **99**, 18447 (1994).
10. S. Manabe and R. Stouffer, personal communication.
11. All solubility model simulations were carried out using the full coupled ocean-atmosphere model. The carbon chemistry was modeled using previously described techniques (19). The air-sea flux of CO_2 was calculated using a wind-speed–dependent gas exchange coefficient [R. Wanninkhof, *J. Geophys. Res.* **97**, 7373 (1992)] multiplied by the air-sea CO_2 difference. The partial pressure of CO_2 in the atmosphere (pCO_2) was specified according to the curves in Fig. 1A. We calculated the surface ocean pCO_2 by solving the full carbon chemistry equations, which required specification of the temperature, salinity, alkalinity, and total carbon content of the ocean. The temperature and salinity were obtained from the models. The alkalinity was modeled in the same way as salinity, with the global mean alkalinity initialized to the observed value. The initial total carbon distribution for the CO_2 uptake simulations was obtained in an ocean-only model by fixing atmospheric pCO_2 at 300 ppm and allowing it to invade the ocean until the ocean was in equilibrium with the atmosphere, that is, the global air-sea flux was zero.
12. The initial condition for the OBM was obtained with the use of an ocean-only model. Formation of organic matter in the surface ocean was determined by forcing the seasonal model surface phosphate toward the observed annual mean phosphate distribution (seasonal data coverage is poor) with a 100-day time scale. Organic carbon formation was calculated using an organic matter C:P ratio of 120. Half of the organic matter formed at the surface was put into particulate matter that is exported to the deep ocean and remineralized instantaneously, following a scaling obtained from sediment-trap

observations [J. H. Martin, G. A. Knauer, D. M. Karl, W. W. Broenkow, *Deep-Sea Res.* **34**, 267 (1987)]. The other half was put into a semilabile dissolved organic carbon pool that decays to inorganic carbon with a mean life of 11.3 years, obtained by requiring that the total semilabile dissolved organic carbon pool remained fixed at its observed value (19). The cycling of $CaCO_3$ was calculated by forcing the horizontally averaged alkalinity profile toward the observed values, after first normalizing both the model and observations to a constant salinity and correcting them for the effect of nitrate cycling. The resulting fits of the model to the annual mean nutrient, carbon, and alkalinity data are very good, and the model has a realistic regional distribution of annual mean air-sea fluxes. The 100-day forcing time scale used to predict surface production of organic matter permits seasonal fluctuations to occur. However, because we used annual mean phosphate observations to determine the new production, the seasonal phosphate and CO_2 fluctuations do not agree very well with seasonal observations in the few regions where such data are available.
13. E. Maier-Reimer, U. Mikolajewicz, A. Winguth, *Clim. Dyn.* **12**, 711 (1996).
14. J. L. Sarmiento and J. R. Toggweiler, *Nature* **308**, 621 (1984).
15. J. L. Sarmiento and J. C. Orr, *Limnol. Oceanogr.* **36**, 1928 (1991).
16. S. W. Chisholm and F. M. M. Morel, Eds., *ibid.*, pp. 1507–1965.
17. A. Neftel, H. Oeschger, J. Schwander, B. Stauffer, R. Zumbrunn, *Nature* **295**, 220 (1982); D. Raynaud *et al.*, *Science* **259**, 926 (1993).
18. R. A. Berner, *Am. J. Sci.* **294**, 56 (1994).
19. J. L. Sarmiento, R. Murnane, C. Le Quéré, *Philos. Trans. R. Soc. London* **348**, 211 (1995).
20. We thank R. Stouffer for assisting us in implementing the coupled model, and both him and S. Manabe for their enthusiastic support and comments on the manuscript. The carbon cycle model was developed by R. Murnane, and both he and R. Slater provided important help interpreting the results. R. Toggweiler, D. Baker, and D. Harvey provided helpful comments on the manuscript. T. Hughes helped analyze the results. We thank J. Mahlman for his comments and the support that the NOAA Geophysical Fluid Dynamics Laboratory has provided for our research over a period of many years through the ocean group headed by R. Toggweiler. Additional support was provided by grants from the NOAA Office of Global Programs, the National Science Foundation, and the Department of Energy.

Red-Emitting Semiconductor Quantum Dot Lasers

S. Fafard,* K. Hinzer, S. Raymond, M. Dion, J. McCaffrey, Y. Feng, S. Charbonneau

Visible-stimulated emission in a semiconductor quantum dot (QD) laser structure has been demonstrated. Red-emitting, self-assembled QDs of highly strained InAlAs have been grown by molecular beam epitaxy on a GaAs substrate. Carriers injected electrically from the doped regions of a separate confinement heterostructure thermalized efficiently into the zero-dimensional QD states, and stimulated emission at $\sim$707 nanometers was observed at 77 kelvin with a threshold current of 175 milliamperes for a 60-micrometer by 400-micrometer broad area laser. An external efficiency of $\sim$8.5 percent at low temperature and a peak power greater than 200 milliwatts demonstrate the good size distribution and high gain in these high-quality QDs.

Semiconductor quantum well laser diodes based on two-dimensional density of states are technologically important because of their high power, high efficiency, and wide tunability (1). Recently, a breakthrough in nano-optics research has permitted the direct growth of semiconductor QDs (2, 3). These QDs have discrete zero-dimensional (0D) energy levels and can be thought of as artificial atoms (4–16). In much the way water vapor condenses into droplets on a piece of glass, in the Stranski-Krastanow growth mode during the molecular beam epitaxy (MBE) of highly strained material, small defect-free islands of uniform size form. If a low band gap semiconductor is embedded in higher band gap material, quantum confinement in all three directions results. This spontaneous island formation has been exploited to produce self-assembled QDs with a variety of III-V semiconductors.

For most materials studied, emission from self-assembled QDs is in the infrared (IR), but radiative recombination in the red part of the visible spectrum has also been achieved (4, 10). These high-quality nanostructures feature a variety of interesting properties such as extremely sharp homogeneous linewidths (4, 5, 7, 10, 14), invariant lifetimes and linewidths for temperatures up to the onset of the thermionic emission (14) state-filling and excited-state emission (6, 8, 12, 13, 16), and distinctive carrier dynamics and phonon interactions (8, 15). Moreover, the one-step in situ fabrication process of these self-assembled QDs makes them technologically compatible with current device structures.

Theory predicts that QD laser structures should have higher gain, lower

Institute for Microstructural Sciences, National Research Council of Canada, Ottawa, Ontario, Canada K1A 0R6.

*To whom correspondence should be addressed.

threshold currents, and a weaker temperature dependence compared with quantum wells. However, more severe energy and momentum conservation rules are imposed by the atomic-like density of states, so carrier injection and thermalization toward the lower states could be less efficient. Carrier relaxation toward the ground states occurs predominantly between levels that are separated by only a few millielectron volts, through longitudinal acoustic phonon emission, or at energies within a few millielectron volts of the longitudinal optical phonon energy. At higher carrier concentrations, relaxation by Coulomb scattering through an Auger-like process has also been considered to play a significant role in the thermalization process (17). This relaxation mechanism is expected to be efficient for dense electron-hole plasmas that are generally present under lasing conditions in semiconductor lasers. Such thermalization processes could therefore be particularly important for small QDs in which the phonon scattering rates might be lower because of the greater intersublevel spacing between the electron or the hole states. For these reasons, structures with QDs have generated interest as a new class of artificially structured materials with tunable energies (by varying the compositions, sizes, and strain of the dots) that are ideal for use in laser structures.

Very recently, InGaAs has been used to produce IR-emitting QD lasers (18–21). For applications requiring shorter wavelengths, emission in the red can be obtained by use of a higher band gap material such as InAlAs. Short-wavelength laser diodes present additional challenges because the available confinement potential between the barriers in the active region and the doped contact layers is reduced. We demonstrate here that red-stimulated emission can be obtained from self-assembled QDs grown in a laser diode cavity. The role of carrier injection in achieving this result is also investigated.

The samples were grown by MBE on an n-doped GaAs(100) substrate. The Stranski-Krastanow growth mode was used to produce one layer of QDs in the active region of a separate confinement heterostructure (Fig. 1, A and B). The structure consists of a thick ($\sim$2 μm) n^+ $Al_{0.33}Ga_{0.67}As$ contact layer, an $Al_{0.30}Ga_{0.70}As$ bottom cladding layer with a lower doping and smaller band gap, and the active region. The active region is made of a 16-nm undoped $Al_{0.25}Ga_{0.75}As$ on each side of the QD layer, which consisted of 4.5 monolayers (ML) of $In_{0.64}Al_{0.36}As$ grown at 530°C. The symmetric step-graded cladding and contact layers with p-doping terminate the structure with a p^+ GaAs cap. A cross-

sectional transmission electron micrograph (TEM) of the active region (Fig. 1C) reveals a relatively high density of InAlAs islands of rounded shape, with a base diameter of $\sim$20 nm and a thickness of $\sim$6.3 $\pm$ 1.0 nm. The morphology is therefore comparable to what has been obtained with other similar self-assembled QDs (10).

The TEM micrograph shows that the growth front returns to a planar mode after only a few nanometers of $Al_{0.25}Ga_{0.75}As$ above the QDs to produce an atomically flat interface at the upper $Al_{0.25}Ga_{0.75}As/Al_{0.30}Ga_{0.70}As$ heterojunction. The p-i-n structure was processed into a broad area laser with two cleaved uncoated facets to form a laser cavity 400 μm in length, with a metallization width of 60 μm. Ohmic contacts were formed on the n^+ and p^+ sides. Under forward bias, as depicted in Fig. 1, A and B, electrons and holes are injected into the QD active region, which results in electroluminescence (EL) or, at high currents, lasing emission (that is, spontaneous

and stimulated emission, respectively).

At 77 K, for very low injection currents, the EL emission is centered at a wavelength λ = 725 nm (1.710 eV) with a Gaussian line shape of $\sim$60 meV at its full width at half maximum (FWHM). This spectrum is similar to the photoluminescence (PL) spectrum (not shown) obtained with nominally equivalent QDs grown in a n-i-n structure designed for a separate optical investigation. It is also comparable to the PL spectra obtained with self-assembled QDs displaying efficient photocarrier thermalization and no observable excited-state emission at low excitation intensity. The inhomogeneously broadened Gaussian EL line shape is therefore attributed to the emission from injected carriers thermalized in the statistically distributed ground states of the probed QD, which vary in energy because of small variations in size, composition, and strain. If we assume a QD coverage of $\sim$50% of the plane (which is roughly that estimated from the TEM cross section), the number of QDs into which carriers are injected is about $\sim$10^7.

With such a large ensemble, it is not possible to observe the very sharp homogeneous EL emission line of each individual QD (4). To reveal the intrinsic sharpness of the emission from each QD, we gated the structure with an opaque electrode with a small (a few square micrometers) opening in its center. The detected EL, which originates from a much smaller number of QDs, is shown in Fig. 2 for various applied voltages. As observed, a number of sharp spectral features of similar amplitude appear with FWHM ranging from 200 to 500 μeV. Each sharp feature corresponds to the EL of a few QDs emitting at similar wavelengths. This demonstrates the 0D-nature of the energy levels in which the electrically in-
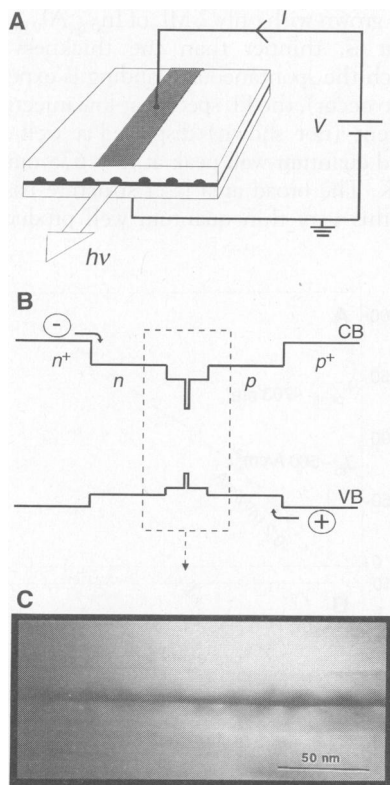
Fig. 1. Schematic view of (**A**) the geometry and (**B**) diagram of the conduction band (CB) and valence band (VB) of a broad area laser diode based on self-assembled semiconductor QDs. The metalization on top of the 400-μm-long cavity is 60 μm wide. The electrons (−) and holes (+) are injected in the active region with a forward voltage (V) and current (I). (**C**) TEM cross-sectional view of the active region, which reveals the $Al_{0.36}In_{0.64}As$ QDs (dark) at the center of the $Al_{0.25}Ga_{0.75}As$ (pale), and with the $Al_{0.25}Ga_{0.75}As/Al_{0.3}Ga_{0.7}As$ interfaces (line above and below).
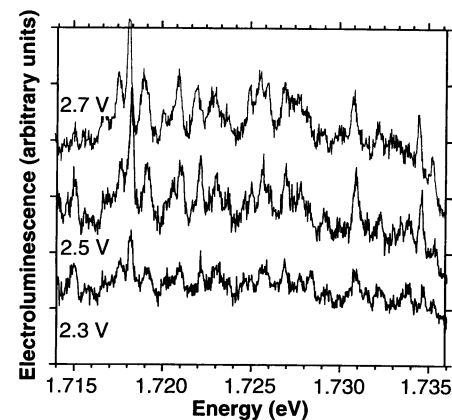
Fig. 2. Low-temperature (4.2 K) EL spectra obtained at various applied voltages on the QD laser sample gated with an opaque electrode having an opening of a few square micrometers that is used to delineate the number of QDs probed. The sharp emission lines reveal the discrete nature of density of states of the individual QDs.

jected carriers thermalize and recombine. The small energy shift of the sharp lines associated with the different biases can be attributed to the quantum-confined Stark effect.

The 77 K emission from the broad area laser structure, driven with forward bias pulses having a duty cycle of a fraction of percent, is shown in Fig. 3. For currents <10 mA, the EL line shape is Gaussian and centered at 725 nm (lowest curve of Fig. 3A). With increasing currents, it becomes asymmetric with a shift of the peak position toward the higher energies. At ~175 mA (current densities $J \sim 700$ A/cm^2), a stimulated emission peak appears on top of the asymmetric EL peak. As the current is increased further, the laser cavity supports multiple longitudinal modes, and several sharp lasing peaks appear near 707 nm (1.754 eV). These can be seen more clearly in the semilogarithmic plot of Fig. 3B for a current of 600 mA ($J = 2500$ A/cm^2) and a peak laser output power of 44 mW.

For each longitudinal mode, a different subset of the QD ensemble provides the optical gain. Also, the ~40-meV blue shift observed between the low-current Gaussian EL spectra and the asymmetric spectra at threshold is most likely attributable to a change from emission from the QD ground states, at low currents, to emission from the QD excited states, at threshold where the

larger number of injected carriers are filling the QD ground states. The 40-meV shift would then correspond to the sum of the electron and the hole intersublevel spacings between two adjacent allowed optical transitions. Similar state-filling effects have been observed in PL spectra of QDs excited optically (8, 12, 13, 16). Furthermore, the side peak observed at $\lambda = 724$ nm (1.713 eV) under lasing conditions (Fig. 3B) matches the peak position of the ground-state emission that is observed at very low injection currents (lowest curve of Fig. 3A). Other devices fabricated from the same wafer gave spectra equivalent to those presented in Fig. 3, including the weaker peak at $\lambda = 725$ nm in the lasing spectra. This result suggests that the stimulated emission at 707 nm originates from the QD excited states and that the weaker peak at 724 nm originates from the filled QD ground states.

The luminescence properties of the QD laser structure can be compared with the emission from samples grown with thinner strained In$_{0.64}$Al$_{0.36}$As layers. For a structure grown with only 2 ML of In$_{0.64}$Al$_{0.36}$As (that is, thinner than the thickness at which the spontaneous islanding is expected to occur), the EL spectra at low injection current (not shown) displayed a well-defined quantum-well peak at $\lambda = 678$ nm at 77 K. The broad area laser structure based on this very thin quantum well produced

stimulated emission at 4 K for an injection current roughly four times greater than that of the QD laser. The stimulated emission originated from the bulk Al$_{0.25}$Ga$_{0.75}$As (at $\lambda = 658$ nm, $h\nu = 1.884$ eV) just above threshold (800 mA) and from the thin quantum well (at $\lambda \sim 670$ nm, $h\nu \sim 1.851$ eV) for higher currents (900 mA).

For currents greater than ~1.2 A, some weak residual QD emission was observed. This suggests that the 2-ML deposition corresponds to the early stages of the island formation where a thin quantum well sprinkled with islands of low density and good uniformity can be expected (2). From its gain properties, we can deduce that another sample with a slightly thicker deposition of 2.5 ML had a higher density of islands. Indeed, the low-current behavior at 4 K for the structure based on a 2.5-ML deposition was similar to that observed with the 4.5-ML laser structure: the spontaneous and stimulated emission were originating from the QDs exclusively with a lasing threshold of ~200 mA. However, the radiative recombination observed at higher temperatures or higher currents, or both, indicates that the injected carriers transit for a relatively longer time in the wetting layer and the bulk Al$_{0.25}$Ga$_{0.75}$As in the case of the 2.5-ML deposition. When the current was increased to 1.5 A at 4 K, in addition to the QD lasing at $\lambda = 703$ nm ($h\nu = 1.764$ eV), weaker peaks originating from the bulk Al$_{0.25}$Ga$_{0.75}$As and from the wetting layer appeared at $\lambda = 670$ and 658 nm, respectively. At 77 K the 2.5-ML sample displayed the QD, wetting layer, and bulk Al$_{0.25}$Ga$_{0.75}$As peaks below threshold. The lasing properties obtained with these thinner In$_{0.64}$Al$_{0.36}$As layers are therefore in contrast to the 4.5-ML QD laser structure for which no bulk or wetting layer emission could be observed for any currents at 4 or 77 K. This result indicates that, if the density of QDs is large enough, all the injected carriers are captured and thermalize efficiently in the QDs.

We investigated the efficiency of the broad area QD laser at 4 K by monitoring the output power emitted from one of the cleaved facets as a function of injected current for pulsed excitation with a duty cycle of a fraction of a percent. Figure 4A shows the output power, and Fig. 4B shows the external efficiency for injection currents up to 2 A. The threshold current was 560 A/cm^2, and the differential efficiency above threshold was 0.2 mW/mA. The one-facet power output reached 200 mW at 1.9 A. From the current-voltage characteristic, a residual series resistance of 1.6 ohms is deduced, so, if we correct for the power loss in this resistance, the net external quantum efficiency (for both facets) is ~8.5%. This result indicates that the inter-
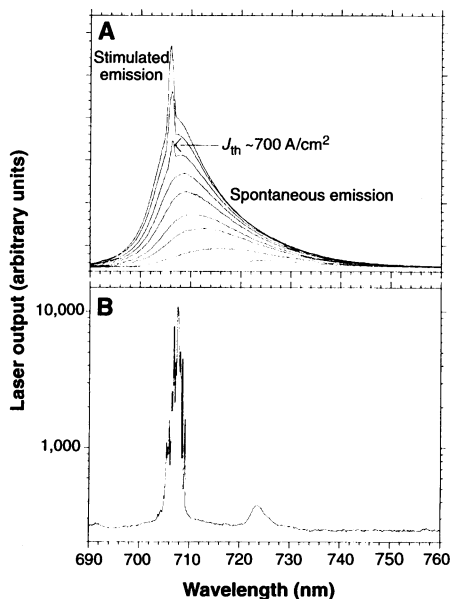
Fig. 3. The (A) EL and (B) multimode lasing spectra at 77 K of the red-emitting InAlAs/AlGaAs QD laser for various forward biases. The emission changes from spontaneous to stimulated as the injection current is increased above a threshold of 175 mA ($J_{th} \sim 700$ A/cm^2). The optical gain for the various lasing modes is provided by a different QD subset in the ensemble of ~10^7 QDs in which carriers are injected.
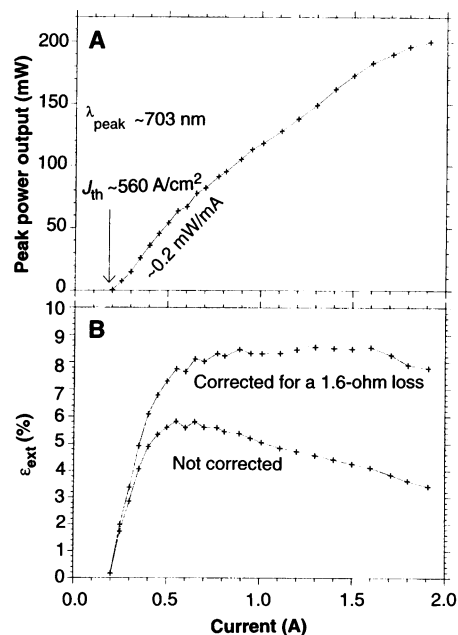
Fig. 4. Lasing properties of the red-emitting QD laser at 4 K as a function of the injection current for forward-bias pulses. (A) Peak power emitted from one facet; (B) two-facet electrical-to-optical conversion efficiency ϵ_{ext} with and without corrections for the power losses in the residual 1.6-ohm contact resistance.

nal gain in the individual QDs is high and that the captures and thermalization of the injected carriers must be efficient because the QD coverage is at most 50% and, because of the inhomogeneous broadening of 60 meV, only a small fraction (estimated to be 5%) of the QDs can emit at the lasing energy. The threshold current density of the QD laser changed little between 4 and 77 K but increased quite rapidly above 80 K. This decrease in the QD laser efficiency at higher temperature is most likely due to a nonoptimized laser design. For example, thermal quenching of the PL in self-assembled QDs is caused by thermionic emission of the carriers above the confining barriers (14). Therefore, an increase in the confinement of the injected carriers that have thermalized in the QDs and in the separate confinement regions of the structures would increase the maximum operating temperature.

The inhomogenous energy broadening associated with the size, composition, and strain variations typical for self-assembled QDs is not too large to destroy the optical gain. With a large enough density of self-assembled QDs, the higher gain associated with the 0D density of states compensates for the unused QDs having an emission energy different from the stimulated emission energy that is supported by the lasing cavity. The 60-meV broadening might therefore offer a wider range of optical gain, which could be exploited in the case of a tunable laser diode structure. Such a uniformity requirement is easily achieved with the spontaneous islanding. However, because of the atomic dimensions involved, it is also unlikely that the present uniformity will be much exceeded. It would be difficult to achieve much higher densities of monochromatic QDs to further improve the conversion efficiency of single-layer QD lasers. However, the prospect of increasing the total number of active QDs by exploiting strain-induced self-organizing mechanisms to grow a stack of several layers of uniform QDs appears to be a promising approach (19–22).

REFERENCES AND NOTES

1. D. Mehuys and D. Evans, *Laser Focus World* **31**, 117 (1995); J. Hecht, *ibid.* **29**, 83 (1993); A. Strass, *ibid.* **30**, 79 (1994).
2. D. Leonard, M. Krishnamurthy, S. Fafard, J. M. Merz, P. M. Petroff, *J. Vac. Sci. Technol. B* **12**, 1063 (1994); D. Leonard, K. Pond, P. M. Petroff, *Phys. Rev. B* **50**, 11687 (1994); D. Leonard et al., *J. Vac. Sci. Technol. B* **12**, 2516 (1994).
3. J. M. Moison et al., *Appl. Phys. Lett.* **64**, 196 (1994).
4. S. Fafard, R. Leon, D. Leonard, J. L. Merz, P. M. Petroff, *Phys. Rev. B* **50**, 8086 (1994); *Superlattices Microstruct.* **16**, 303 (1994); S. Fafard, D. Leonard, J. L. Merz, P. M. Petroff, *Appl. Phys. Lett.* **65**, 1388 (1994).
5. J.-Y. Marzin, J.-M. Gérard, A. Izraël, D. Barrier, G. Bastard, *Phys. Rev. Lett.* **73**, 716 (1994).
6. H. Drexler, D. Leonard, W. Hansen, J. P. Kottaus, P. M. Petroff, *ibid.*, p. 2252.
7. M. Grundmann et al., *ibid.* **74**, 4043 (1995); M. Grundmann et al., *Phys. Status Solidi* **188**, 249 (1995).
8. S. Fafard, R. Leon, D. Leonard, J. L. Merz, P. M. Petroff, *Phys. Rev. B* **52**, 5752 (1995); S. Raymond et al., *ibid.*, p. 17238.
9. R. Nötzel et al., *Appl. Phys. Lett.* **66**, 2525 (1995).
10. R. Leon, P. M. Petroff, D. Leonard, S. Fafard, *Science* **267**, 1966 (1995); R. Leon, S. Fafard, D. Leonard, J. L. Merz, P. M. Petroff, *Appl. Phys. Lett.* **67**, 521 (1995).
11. K. Imamura et al., *Jpn. J. Appl. Phys. A* **11**, L1445 (1995).
12. S. Fafard, Z. Wasilewski, J. McCaffrey, S. Raymond, S. Charbonneau, *Appl. Phys. Lett.* **68**, 991 (1996).
13. M. Grundmann et al., *ibid.*, p. 979.
14. S. Fafard et al., *Surface Sci.* **361–362**, 778 (1996).
15. R. Heitz et al., *Appl. Phys. Lett.* **68**, 361 (1996).
16. S. Raymond et al., *Phys. Rev. B* **54**, 11548 (1996).
17. U. Bockelmann and G. Bastard, *ibid.* **42**, 8947 (1990); U. Bockelmann and T. Egeler, *ibid.* **46**, 15574 (1992); U. Bockelmann, *ibid.* **48**, 17637 (1993).
18. K. Kamath, P. Bhattacharya, T. Sosnowski, T. Norris, J. Phillips, *Electron. Lett.* **32**, 1374 (1996).
19. H. Shoji et al., *IEEE Photonics Technol. Lett.* **7**, 1385 (1995); H. Shoji et al., *Jpn. J. Appl. Phys. II, Lett.* **35**, L903 (1996).
20. Z. I. Alferov et al., *Semiconductors* **30**, 194 (1996); O. G. Schmidt et al., *Electron. Lett.* **32**, 1302 (1996). N. Kirstaedter et al., *ibid.* **30**, 1416 (1994).
21. Q. Xie, A. Kalburge, P. Chen, A. Madhukar, *IEEE Photonics Technol. Lett.* **8**, 965 (1996).
22. J. Tersoff, C. Teichert, M. G. Lagally, *Phys. Rev. Lett.* **76**, 1675 (1996).
23. We thank Z. Wasilewski, P. Hawrylak, P. T. Coleridge, and P. Corkum for helpful discussions. The technical assistance of J. Stapledon, P. Chow-Chong, P. Marshall, and A. Golsham is also acknowledged.

Chemiluminescence in the Agglomeration of Metal Clusters

L. König, I. Rabin, W. Schulze, G. Ertl*

The agglomeration of copper or silver atoms in a matrix of noble gas atoms to form small clusters may be accompanied by the emission of visible light. Spectral analysis reveals the intermediate formation of electronically excited atoms and dimers as the source of the chemiluminescence. A mechanism is proposed, according to which the gain in binding energy upon cluster formation may even lead to the ejection of excited fragments as a result of unstable intermediate configurations. A similar concept was introduced in the field of nuclear reactions by Niels Bohr 60 years ago.

Exothermic chemical reactions may be accompanied by chemiluminescence. In these reactions, the released energy is not adiabatically damped into the heat bath of the surrounding medium but rather is stored in an excited state of the product; decay from this excited state to the ground state is associated with light emission. In the course of our studies into the formation of metal clusters, we discovered, under specific conditions, the emission of visible light, as well as evidence for the production of electronically excited atoms and dimers.

The effect was discovered in an experimental arrangement comprising a cluster source based on the gas aggregation technique. Metal atoms thermally evaporated from a Knudsen cell are transported by a stream of noble gas into a nucleation zone, where cooling of the gas stream by the cold walls leads to homogeneous nucleation and growth of clusters. The cluster size distribution can be varied from 2 (dimers) to about 10^4 atoms per cluster (1) by changing the experimental conditions. The clusters leaving the source together with large quantities of the carrier gas can be subjected to various experiments and are eventually trapped at the walls of a cryopump cooled by liquid He, where a cluster-doped noble gas matrix is formed at high deposition rates.

In the course of such experiments with small clusters of Cu, Ag, or Au, the emission of light from the growing layers was visually observed under specific conditions. The intensity depended on matrix temperature and metal concentration.

To study these effects in detail, we modified the cluster source to allow the formation of matrices on a quartz window of a cryostat with an unusually high gas deposition rate (about 10^{18} atoms s^{-1} cm^{-2}) and with a gas-to-metal ratio exceeding 5000. The growth rate of the matrix was about 1 cm hour^{-1}, so that rather thick layers were formed. As a consequence, the gas loss due to re-evaporation was negligible during warm-up experiments, even at 50 K. Under these operating conditions, mainly atoms and dimers are produced by the cluster source. The emitted light was analyzed by a monochromator coupled to a CCD (charge-coupled device) detector system. Possible influences by spurious effects were carefully checked: We eliminated the possibility of energy supply by electrons or ions from the

Fritz-Haber-Institut der Max-Planck-Gesellschaft, Faradayweg 4-6 (Dahlem), D-14195 Berlin, Germany.

*To whom correspondence should be addressed. E-mail: ertl@fhi-berlin.mpg.de